Chapter 5

Formation of primordial stars in a WDM universe

5.1 Summary

In this chapter I discuss aspects of primordial star formation in a universe with a generic warm dark matter (WDM) cosmology. After describing the theory and general effects of a warm dark matter power spectrum, I compare the results of simulations done with a single cosmological realization but using a wide range of warm dark matter particle masses which have not yet been ruled out by observation. The main effect of the WDM is that the addition of a warm dark matter component to the initial power spectrum results in a delay in the collapse of the gas at the center of the halo which forms a primordial protostar and an increase in the virial mass of the halo at the onset of collapse. Both of these effects become more pronounced as the WDM particle mass becomes smaller. A cosmology using a warm dark matter spectrum assuming a particle mass of $m_{WDM} \simeq 40$ keV is effectively indistinguishable from the cold dark matter case, and a reasonable lower limit to a warm dark matter particle mass of $\simeq 15$ keV is suggested in order for Population III stars to contribute significantly to the polarization result observed by the WMAP satellite. There is remarkably little scatter in the final properties of the primordial protostar which forms at the center of the halo, possibly due to the overall low rate of halo mergers which is a result of the WDM power spectrum. I also describe the detailed evolution of the collapsing halo core in two representative WDM cosmologies. Once the gas in the center of the halo reaches relatively high densities ($n \sim 10^5$ cm^{-3}), the overall evolution is essentially identical in the two calculations.

5.2 Motivation and theory

As discussed in Section 1.5, there are some apparent flaws in the ΛCDM paradigm at small scales. These include a lack of observation of dark matter "cusps," which are predicted by theory and numerical simulations in the CDM universe, the absence of the very large number of dwarf galaxies predicted by the cold dark matter paradigm, and others. However, at large scales (greater than 1 megaparsec or so) the CDM model seems to describe the evolution of the universe and the structure within it incredibly well. The problem, therefore, is to come up with some physical explanation for the apparent lack of power on small scales while retaining the desirable qualities of the CDM model on large scales.

Many models have been proposed that do this, with a wide variety of mechanisms. A generic feature of these models is that they suppress the cosmological power spectrum on small scales, while leaving large scales alone. In this chapter I will discuss the ramifications of the most general possible model, referred to as "warm dark matter." The effects of a general warm dark matter cosmology are discussed by Bode, Ostriker & Turok [115], who derive the relevant linear perturbation theory and perform several N-body calculations of warm dark matter cosmologies to understand the general effects of suppression of power on small scales. They find that replacing cold dark matter with warm dark matter results in the smoothing of massive halo cores, which lowers core densities and increases core radii, lowers the characteristic density of low-mass halos, reduces the overall total number of low-mass halos, suppresses the number of low-mass satellite halos in high-mass halos, and results in the formation of low-mass halos almost entirely within caustic sheets or filaments connecting larger halos – voids are almost completely empty, in contrast to CDM. They also find that low-mass halos tend to form at late times, in a top-down process (as opposed to the bottom-up process of halo formation one would expect from a CDM cosmology), and that halo formation is suppressed overall at early times (high redshift), with an increased evolution of halos at low redshifts relative to the CDM model. Furthermore, they suggest that a reasonable minimum warm dark matter particle mass would be 1 keV.

Other constraints on the minimum mass of a warm dark matter particle have been placed by various groups. Barkana, Haiman & Ostriker [212] use an extended Press-Schechter model to constrain warm dark matter based on constraints from cosmological reionization. They calculate that in order for super massive black holes to exist at $z \simeq 6$, and if massive galaxies are responsible for the nearly complete reionization of the universe by the same redshift, a reasonable minimum mass for a warm dark matter particle is $m_{WDM} \geq 1.2$ keV. Dalal & Kochanek [213] show that constraints on small-scale linear power using strong gravitational lensing find agreement with agreement with ΛCDM models, and place a minimum bound on a possible warm dark matter mass of $m_{WDM} > 5.2$ keV. Additionally, Yoshida et al. perform a SPH cosmological simulation of

structure formation in the early universe assuming a WDM particle mass of 10 keV. They find that this calculation is inconsistent with the high Thomson optical depth observed by the WMAP satellite, and suggest that any successful WDM model will have a particle mass greater than 10 keV [214].

Bode et al. derive a formula for the power spectrum cutoff due to the existence of a generic warm dark matter particle. They provide the following transfer function that models the smoothing of small-scale density perturbations:

$$T_k^X = [1 + (\alpha k)^2]^{-5} \tag{5.1}$$

Where $\alpha = 0.05(\Omega_x/0.4)^{0.15}(h/0.65)^{1.3}(keV/m_X)^{1.15}(1.5/g_x)^{0.29}$ and k is in units of h Mpc^{-1}. In this equation Ω_X is the contribution of the warm dark matter species to the energy density of the universe, in units of the critical density, m_X is the WDM particle mass in keV, h is the Hubble constant in units of 100 km/s/Mpc, and g_x is a parameter meant to represent the effective number of relativistic species present at decoupling, and is taken to be 1.5 for light neutrinos. This is considered to be the fiducial value for g_x for the warm dark matter particle. This transfer function corresponds to a strong rollover in the power spectrum, corresponding to a smoothing scale of:

$$R_s \simeq 0.31 \left(\frac{\Omega_x}{0.3}\right)^{0.15} \left(\frac{h}{0.65}\right)^{1.3} \left(\frac{keV}{m_X}\right)^{1.15} h^{-1}Mpc \tag{5.2}$$

This smoothing scale corresponds to the comoving half-wavelength of the mode for which the linear perturbation amplitude is suppressed by a factor of 2. This results in a characteristic mass scale below which structure forms by the top-down fragmentation of halos, rather than by the bottom-up hierarchical structure formation associated with the cold dark matter paradigm. This mass scale can be quantified as:

$$M_s = 10^{10} \left(\frac{\Omega_x}{0.3}\right)^{1.45} \left(\frac{h}{0.65}\right)^{3.9} \left(\frac{keV}{m_X}\right)^{3.45} h^{-1}M_\odot \tag{5.3}$$

Figure 5.1 contains several panels demonstrating the effects of the warm dark matter cosmology discussed above. The top left panel shows the cosmological power spectrum $P(k)$ at $z = 0$ for a CDM cosmology as well as for when the WDM transfer function has been applied for several different warm dark matter masses ranging from $0.1 - 100$ keV. The top right panel shows the dimensionless linear power $\Delta^2(k) \sim k^3P(k)$ with the same particle masses. The bottom left panel shows the suppression mass as a function of radius, and the bottom right panel shows the comoving smoothing scale. In the bottom two panels the red dashed line indicates the mass and radius corresponding to a halo of mass 4×10^5 $\mathrm{M}_\odot$, which is approximately the mean halo mass of all of the CDM simulations discussed in Chapter 4. This mass scale corresponds to a WDM particle mass of ~ 15 keV.

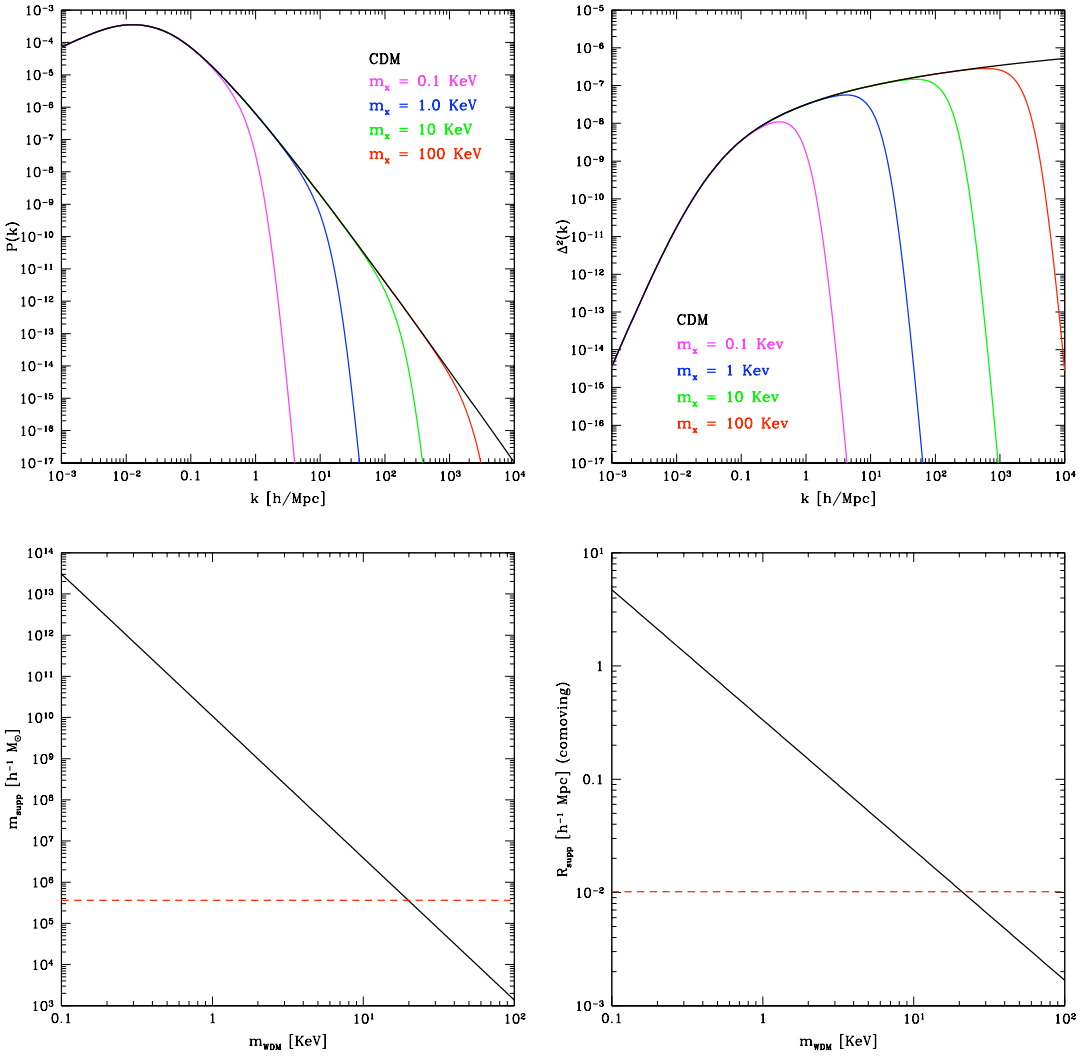

Figure 5.1: Plots showing various effects of a generic warm dark matter particle. Top left panel: The dark matter power spectrum $P(k)$ as a function of wavenumber $k \equiv 2\pi/\lambda$ for a CDM cosmology and a range of warm dark matter masses. Top right panel: The dimensionless power, $\Delta^2(k) \sim k^3 P(k)$, versus k. Bottom left panel: The "suppression mass" as a function of WDM particle mass. Bottom right panel: The "smoothing scale" as a function of WDM particle mass. In the bottom two plots the red dashed line indicates the mass and radius corresponding to a halo of mass 4×10^5 $M_\odot$, which is approximately the mean halo mass from the simulations discussed in Chapter 4.

5.3 Problem setup

The simulations discussed in this chapter use a similar setup to those in Chapter 4. A single cosmological realization in a box size of 0.3 h^{-1} Mpc is chosen at random from the four available CDM calculations. This calculation is initialized at $z = 99$ assuming a "concordance" cosmological model: $\Omega_m = 0.3$, $\Omega_b = 0.04$, $\Omega_{DM} = 0.26$, $\Omega_\Lambda = 0.7$, $h = 0.7$ (in units of 100 km/s/Mpc), $\sigma_8 = 0.9$, and using an Eisenstein & Hu power spectrum [194] with a spectral index of $n = 1$. At this point, we generate several sets of initial conditions with the same large-scale structure by smoothing the CDM initial conditions with the warm dark matter transfer function described in Equation 5.1, assuming $\Omega_x = \Omega_{DM} = 0.26$, $g_x = 1.5$, and warm dark matter masses of $m_x = 10, 12.5, 15, 17.5, 20, 25, 30, 35$, and 40 keV. The initial conditions are generated with both dark matter and baryons such that the Lagrangian volume in which the halo in the CDM case formed is resolved at high spatial and mass resolution using the nested initial condition method described in Section 2.1.2, with a 128^3 root grid and three static nested grids, for an overall effective grid size of 1024^3. The highest resolution grid is 256^3 grid cells, and corresponds to a volume 75 h^{-1} comoving kpc on a side. The dark matter particles in the highest resolution grid are 1.81 h^{-1} $M_\odot$ and the spatial resolution of the highest resolution grid is 293 h^{-1} parsecs (comoving). Previous work shows that this particle mass resolution is more than adequate to fully resolve the collapse of the halo.

All simulations are performed using the adaptive mesh cosmology code Enzo, described in detail in Section 2.2. The simulations are started at $z = 99$ and allowed to evolve until the collapse of the gas within the center of the most massive halo, which occurs at a range of redshifts. The equations of hydrodynamics are solved using the PPM method with a dual energy formulation, as described in Section 2.2.2. The nonequilibrium chemical evolution and optically thin radiative cooling of the primordial gas is modeled as described in Section 2.2.5, following 9 separate species including molecular hydrogen (but excluding deuterium). Adaptive mesh refinement is used such that cells are refined by factors of two along each axis, with a maximum of 22 total levels of refinement. This corresponds to a maximum spatial resolution of 115 h^{-1} astronomical units (comoving) at the finest level of resolution, with an overall spatial dynamical range of 5.37×10^8. To avoid effects due to the finite size of the dark matter particles, the dark matter density is smoothed on a comoving scale of ~ 0.5 pc. This is reasonable because at that radius in all of our calculations the gravitational potential is dominated by the baryons.

Grid cells are adaptively refined based upon several criteria: baryon and dark matter overdensities in cells of 4.0 and 8.0, respectively, as well as criteria to ensure that the pressure jump and/or energy ratios between adjoining cells never exceeds 5.0, that the cooling time in a given cell is always longer than the sound crossing time of that cell, and that the Jeans length is always resolved by at least 16 cells. This guarantees that the Truelove criterion [217] is always maintained by a comfortable margin.

5.4 Results

5.4.1 Comparison of realizations with many WDM particle masses

In this section we discuss the results of a comparison of all of the WDM simulations, along with the cold dark matter "control" simulation. Figure 5.2 shows bulk properties of the halo in which the Population III protostar forms as a function of the warm dark matter particle mass. The top left and right panels plot the WDM particle mass versus the redshift at which the halo core collapses. The CDM result in each case is shown by a vertical blue line. These panels demonstrate that decreasing the warm dark matter particle mass delays the formation of the protostar. The 40 keV calculation forms at essentially the same time as the CDM simulation, while collapse of the halo core in the calculation assuming a 12.5 keV WDM particle mass is delayed by approximately 130 million years. The simulation with a 10 keV particle mass does not collapse by $z = 10$ (the end of the simulation) and is not shown here. The delay of the halo collapse appears to be smoothly varying as a function of WDM particle mass.

The bottom panel of Figure 5.2 shows the virial mass of the halo (at the redshift of collapse) as a function of WDM particle mass. A reduction in the WDM particle mass leads to an increase in the halo virial mass, which is related to the delay in collapse of the halo core – by the time the halo core collapses in the lower particle mass simulations, the halo has had time to accrete more mass.

Figures 5.3 and 5.4 show several spherically-averaged, mass-weighted radial profiles of baryon quantities as a function of radius or enclosed mass of the simulations. All profiles are taken at a constant point in the evolution of the protostellar cloud (when the central number density is $n \sim 10^{10}$ cm^{-3}) rather than at a constant point in time, since the halos collapse over a wide range of redshifts. Figure 5.3 shows the baryon number density as a function of enclosed mass (top left panel), baryon temperature as a function of enclosed mass (top right panel), molecular hydrogen fraction as a function of enclosed mass (bottom left panel), and enclosed mass as a function of radius (bottom right panel). As expected, the number density profiles of all of the simulations are very similar over the entire range of WDM (and CDM) particle masses. This is a result of the cooling properties of a gas of primordial composition, as explained in Chapter 4. The simulation assuming a WDM particle mass of 10 keV does not collapse by the time the simulation is stopped at $z = 10$, and the density profile at the last output time is shown. The plot of enclosed mass as a function of radius shows a strong similarity between the different calculations as well, which is to be expected since it is essentially another way of viewing the number density plot. The plots of temperature and molecular hydrogen fraction vs. enclosed mass show a significant amount of scatter. Ignoring the 10 keV case, the overall spread in temperature in the core of the halo is a factor of ~ 3 and the spread in molecular hydrogen fraction is roughly 1.5 orders of magnitude. Interestingly

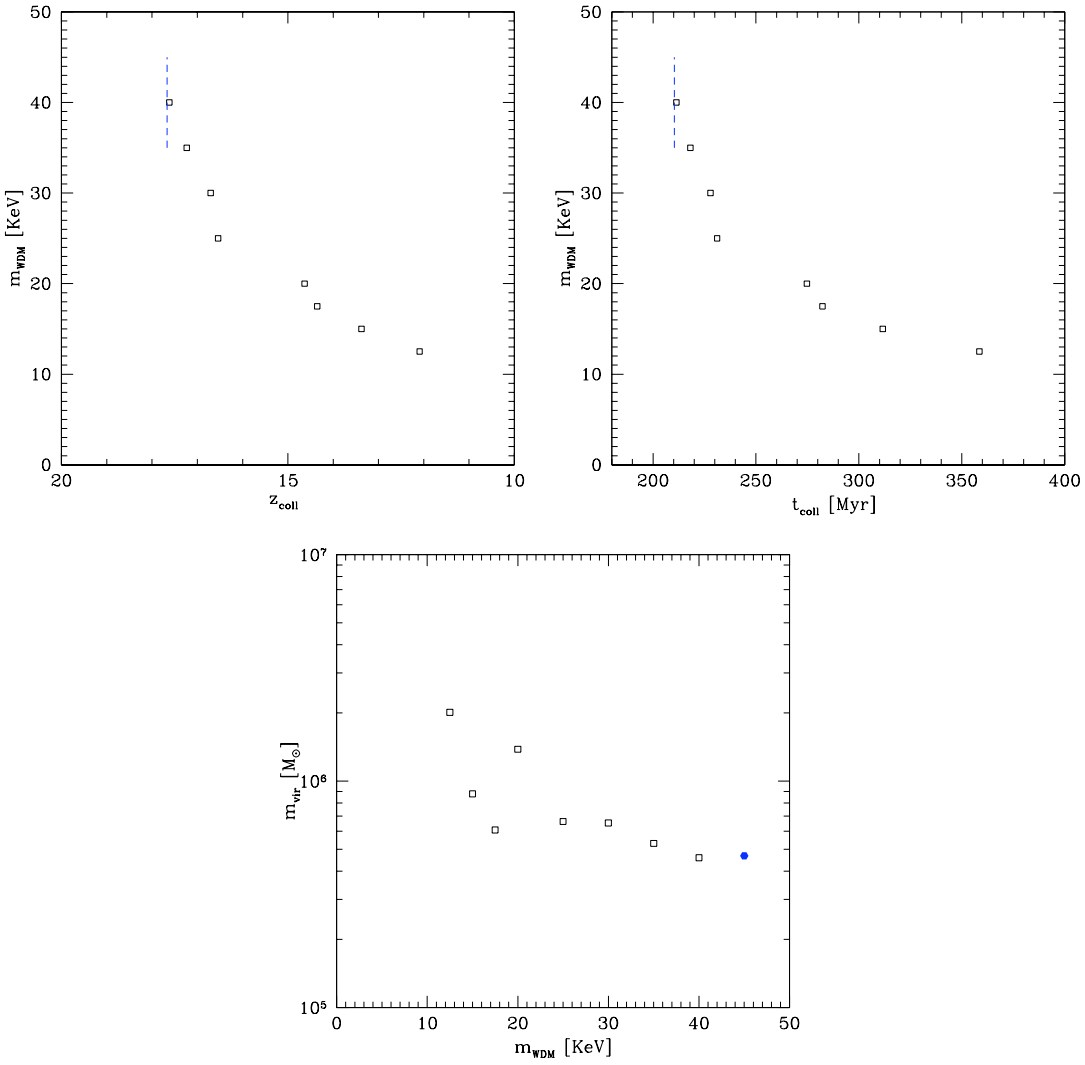

Figure 5.2: Dark matter halo properties as a function of WDM particle mass for several simulations with the same cosmological realization but different warm dark matter particle masses. Top left: WDM particle mass vs. collapse redshift of halo core. Top right: WDM particle mass vs. collapse time of halo core (measured in millions of years after the big bang). Bottom: halo virial mass at collapse vs. WDM particle mass. In the top two panels the collapse redshift/time of the cold dark matter (CDM) simulation is shown by a vertical, dashed blue line. In the bottom panel the virial mass of the halo in the CDM simulation is shown by a solid blue circle, while the WDM simulations are represented by open black squares.

enough, the CDM "control" simulation has one of the higher core temperatures.

Figure 5.4 shows the specific angular momentum as a function of enclosed mass (top left panel), circular velocity as a function of radius (top right panel), radial velocity as a function of enclosed mass (bottom left panel), and accretion time as a function of enclosed mass (bottom right panel). The angular momentum distributions are extremely similar for all of the calculations (disregarding the 10 keV case since it does not collapse), as is the circular velocity. The Keplerian orbital velocity is plotted in this panel (upper thin black line), and all of the simulations display circular velocities that are significantly below this velocity. The plot of radial velocity as a function of enclosed mass shows that the CDM simulation has the greatest infall velocity at the output time in question, which corresponds to the largest accretion rate overall (as shown in the plot of accretion time vs. enclosed mass). The rest of the calculations have similar infall velocities and accretion rates, except for the 15 keV model, which has a much lower overall infall velocity and accretion rate. The reason for this is not obvious at the present time. The overall accretion rates for the WDM calculations are slightly less than that of the CDM calculation, suggesting that the final stellar masses may be slightly lower.

5.4.2 Comparison of the evolution of two representative WDM realizations

In this section we compare the evolution of two representative warm dark matter simulations. We somewhat arbitrarily choose the calculations with WDM particle masses of 12.5 and 25 keV. Figures 5.5 shows mass-weighted projections of dark matter density, baryon density, and baryon temperature at $z = 20.38$ for the two representative WDM calculations and a CDM calculation of the same cosmological realization. All panels show a volume that is ~ 300 pc (proper) across and are centered on the point in space where the first Population III protostar will form. There is a huge difference between the calculations at a fixed point in time – the cold dark matter calculation (right column) shows a great deal of clumpy dark matter structure, including knots along the cosmological filaments and even dark matter halos in void regions, with corresponding variety in the baryon density and temperature plots. The 25 keV calculation shows the effects of smoothing - two halos are forming, but there are no halos in the voids, and no substructure around the halos that form. This is reflected in the baryon temperature and density plots, where the accretion shocks onto the filaments show little small-scale structure and the gas is quite smooth. The 12.5 keV calculation is an even more striking example of the effects of small-scale smoothing – though an overdensity in the dark matter is apparent, no halos are visible at this redshift and there is no smaller scale structure whatsoever. This particle mass corresponds to a smoothing scale of a few times 10^6 $M_\odot$, below which top-down fragmentation takes place. This mass is roughly equivalent to the coalescing halo shown in this image.

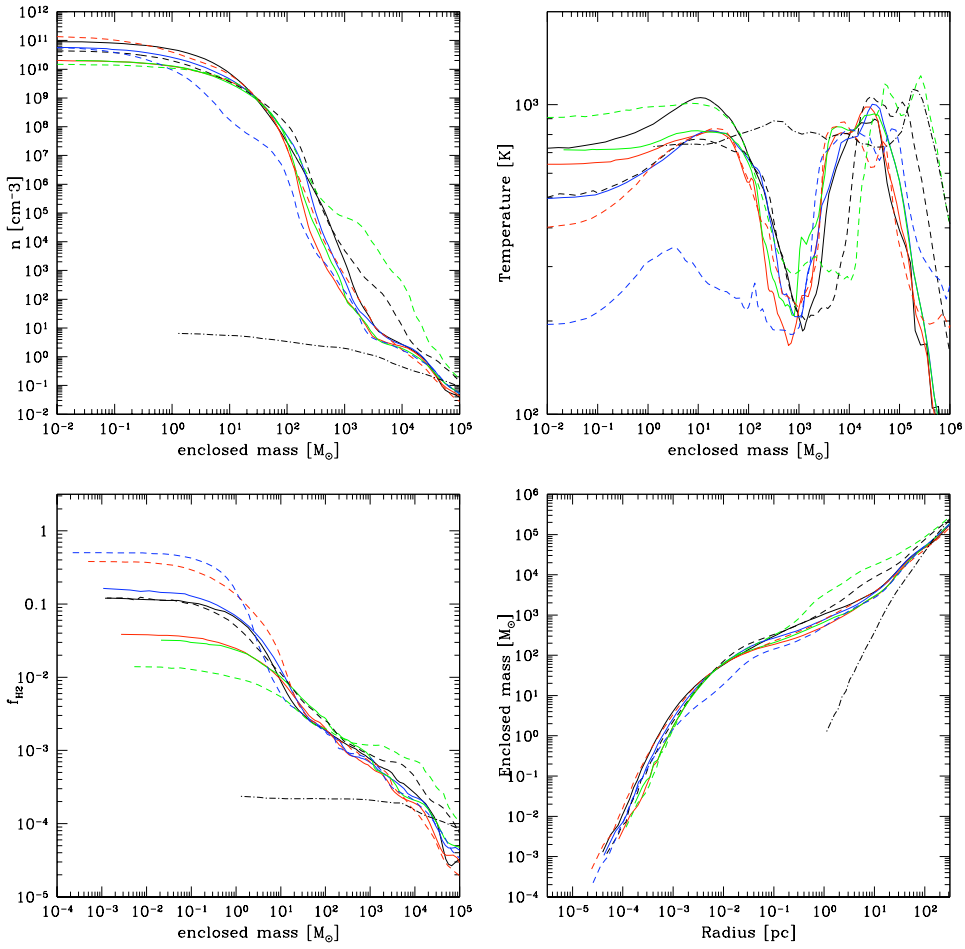

Figure 5.3: Mass-weighted, spherically-averaged baryon quantities for several simulations with the same cosmological realization but different warm dark matter particle masses. Top left: baryon number density as a function of enclosed mass. Top right: baryon temperature as a function of enclosed mass. Bottom left: molecular hydrogen fraction as a function of enclosed mass. Bottom right: enclosed baryon mass as a function of radius. Output times are chosen such that the peak baryon density in each simulation is approximately the same. In each panel, the CDM simulation is represented by a solid black line. Solid red line: $M_{WDM} = 35$ keV. Solid blue line: $M_{WDM} = 30$ keV. Solid green line: $M_{WDM} = 25$ keV. Dashed black line: $M_{WDM} = 20$ keV. Dashed red line: $M_{WDM} = 17.5$ keV. Dashed blue line: $M_{WDM} = 15$ keV. Dashed green line: $M_{WDM} = 12.5$ keV. Dot-dashed black line: $M_{WDM} = 10$ keV. The halo in the $M_{WDM} = 10$ keV does not collapse by the end of the simulation and is shown at the last available output time.

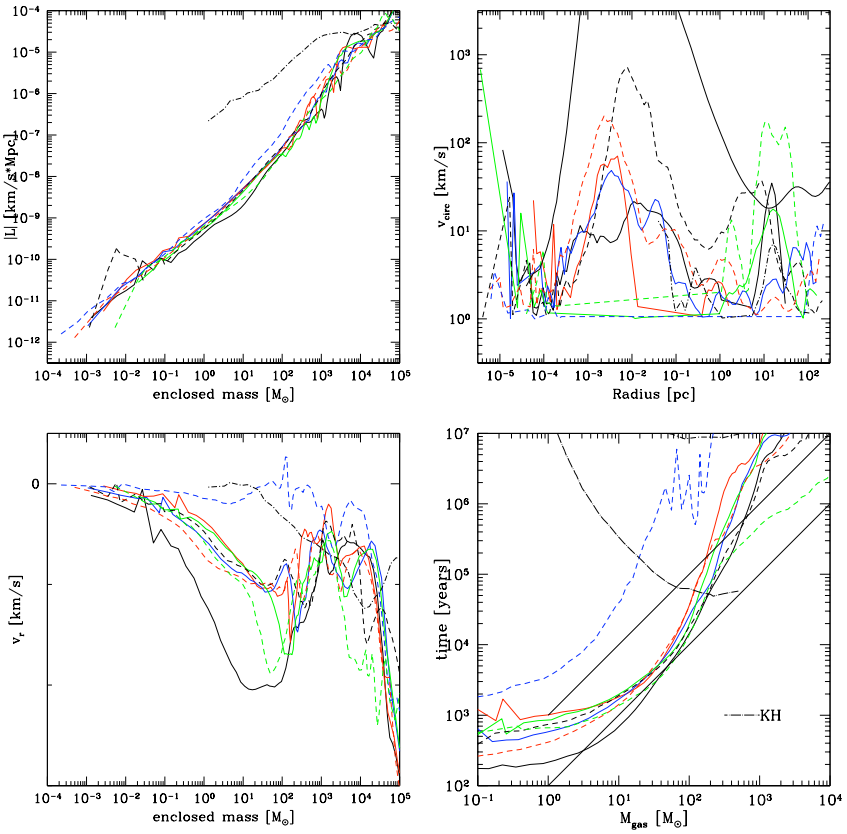

Figure 5.4: Mass-weighted baryon quantities for several simulations with the same cosmological realization but different warm dark matter particle masses. Top left: spherically-averaged baryon angular momentum as a function of enclosed mass. Top right: cylindrically-averaged circular velocity a function of radius. Bottom left: spherically-averaged radial velocity as a function of enclosed mass. Bottom right: spherically-averaged accretion rate as a function of enclosed mass. Output times are chosen such that the peak baryon density in each simulation is approximately the same. In each panel, the CDM simulation is represented by a solid black line. Solid red line: $M_{WDM} = 35$ keV. Solid blue line: $M_{WDM} = 30$ keV. Solid green line: $M_{WDM} = 25$ keV. Dashed black line: $M_{WDM} = 20$ keV. Dashed red line: $M_{WDM} = 17.5$ keV. Dashed blue line: $M_{WDM} = 15$ keV. Dashed green line: $M_{WDM} = 12.5$ keV. Dot-dashed black line: $M_{WDM} = 10$ keV. The halo in the $M_{WDM} = 10$ keV does not collapse by the end of the simulation and is shown at the last available output time. In the bottom right panel the dot-long dashed line is the Kelvin-Helmholz time calculated from Population III stellar properties from Schaerer and the upper and lower diagonal solid black lines correspond to constant accretion rates of 10^{-3} and 10^{-3} $M_{\odot}$/yr, respectively.

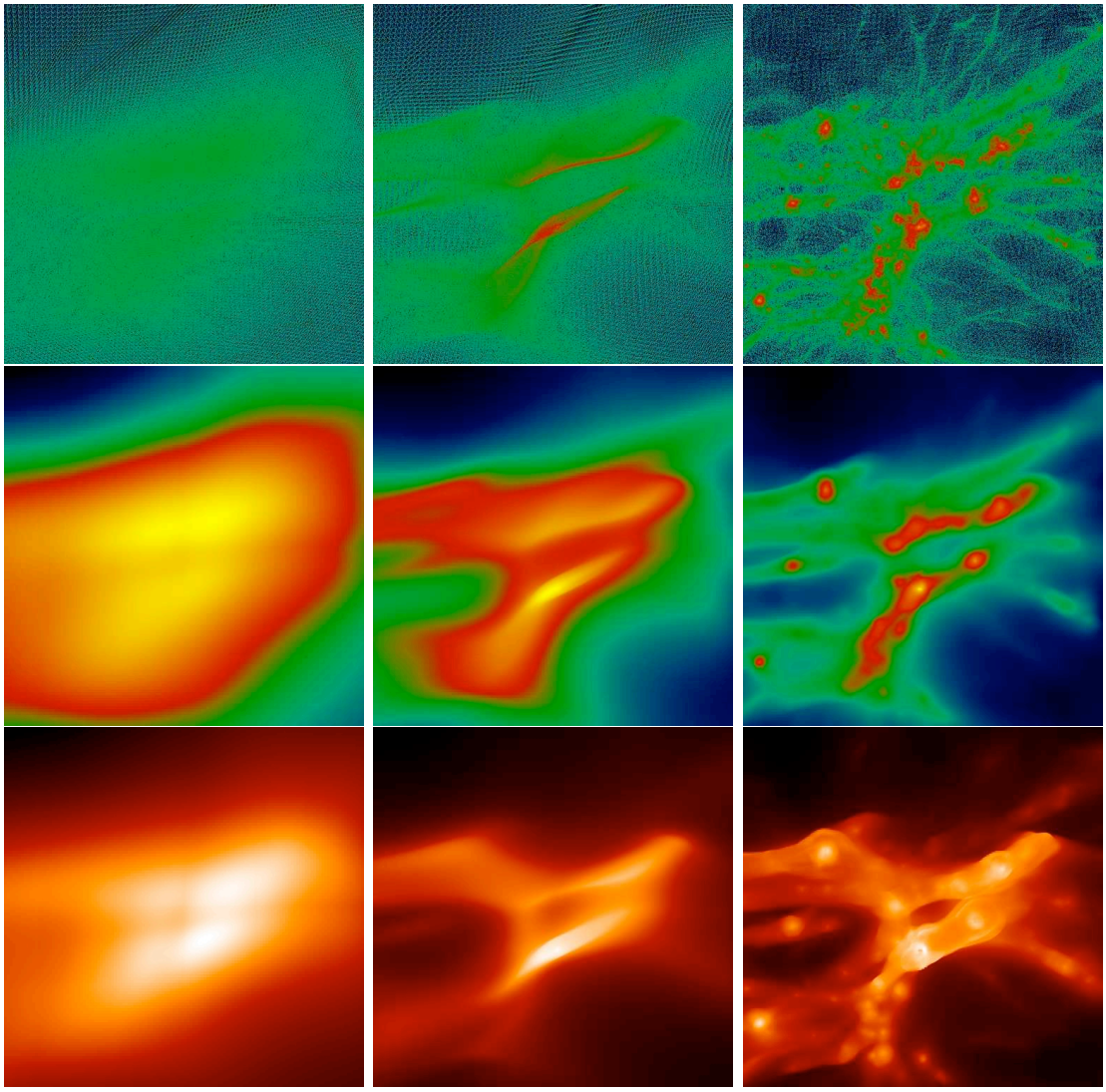

Figure 5.5: Mass-weighted projections of dark matter density, baryon density and baryon temperature for 3 simulations with the same cosmological realization and a range of warm dark matter (WDM) particle masses at $z = 20.38$. The field in each calculation is the same, though the color tables are relative for each panel in order to highlight density differences. Left column: $M_{WDM} = 12.5$ keV. Center column: $M_{WDM} = 25$ keV. Right column: Cold dark matter realization (corresponds to $M_{WDM} \rightarrow \infty$). Top row: projected dark matter density. Middle row: projected baryon density. Bottom row: projected baryon temperature. The spatial scale is ~ 300 pc (proper) in each volume.

Figure 5.6 shows the same quantities and spatial volume as Figure 5.5, though instead of the outputs all being at the same point in time, they are at the time when the halo core collapses in each simulation. This corresponds to $z = 18.001$ for the CDM calculation, $z = 16.54$ for the WDM calculation with $m_{WDM} = 25$ keV, and $z = 12.09$ for the WDM calculation with $m_{WDM} = 12.5$ keV. At the time of collapse the 12.5 keV calculation has formed a halo which is more massive than the CDM halo by a factor of ~ 5 (and collapses approximately 130 million years later). Very little substructure is evident in the projected dark matter distribution of the 12.5 keV calculation. Some is apparent in the 25 keV run, but not nearly as much as in the CDM calculation. As predicted by Bode et al., the warm dark matter calculations have suppressed substructure and satellite halos, and there is significant evidence that the halo in the 12.5 keV calculation forms by top-down fragmentation of a filament rather than hierarchical merging of smaller halos.

Figures 5.7 through 5.9 show the time evolution of several spherically averaged, mass-weighted radial quantities for the two representative warm dark matter calculations. The CDM run is the one discussed in Section 4.4.1, and its evolution is shown in Figures 4.4 through 4.8. The plots are chosen such that the central densities of the collapsing halo core are matched between the two calculations.

Figure 5.7 shows the evolution of number density as a function of enclosed mass for the 12.5 keV and 25 keV WDM calculations. The lowest-density line corresponds to $z = 13.16$ for the 12.5 keV run and $z = 18.05$ for the 25 keV calculation. Intriguingly, it takes the 12.5 keV calculation about 4×10^7 years to advance to a core baryon number density of $n \sim 10^6$ cm^{-3}, while the 25 keV calculation only requires $\sim 2 \times 10^7$ years to get to that point. However, once the calculations reach $\sim 10^6$ cm^{-3} they take extremely similar amounts of time to evolve to the highest number density shown. As discussed in previous sections, this reflects the fact that the halo evolution on small scales is controlled by the chemistry and cooling properties of the primordial gas, which is the same in the two calculations.

Figure 5.8 shows the evolution of baryon temperature and molecular hydrogen fraction as a function of enclosed mass for the two WDM simulations. The overall temperature evolution is very similar between the two calculations, though the calculation with $m_{WDM} = 12.5$ keV ends up with a slightly lower molecular hydrogen fraction and slightly higher central temperature. The evolution of radial infall velocity and angular momentum as a function of enclosed mass (shown in Figure 5.9) is also quite similar between the two calculations. As shown in Figure 5.4, the final accretion rates are also essentially the same.

The purpose of this section was to demonstrate that the evolution of the halo collapse, and the resulting protostar, is quite similar for two simulations with significantly different warm dark matter particle masses. The large-scale structure evolves somewhat differently in these two cases – the halo that forms in the 12.5 keV calculation is approximately the same mass scale as the suppression mass, meaning that this dark matter halo is roughly

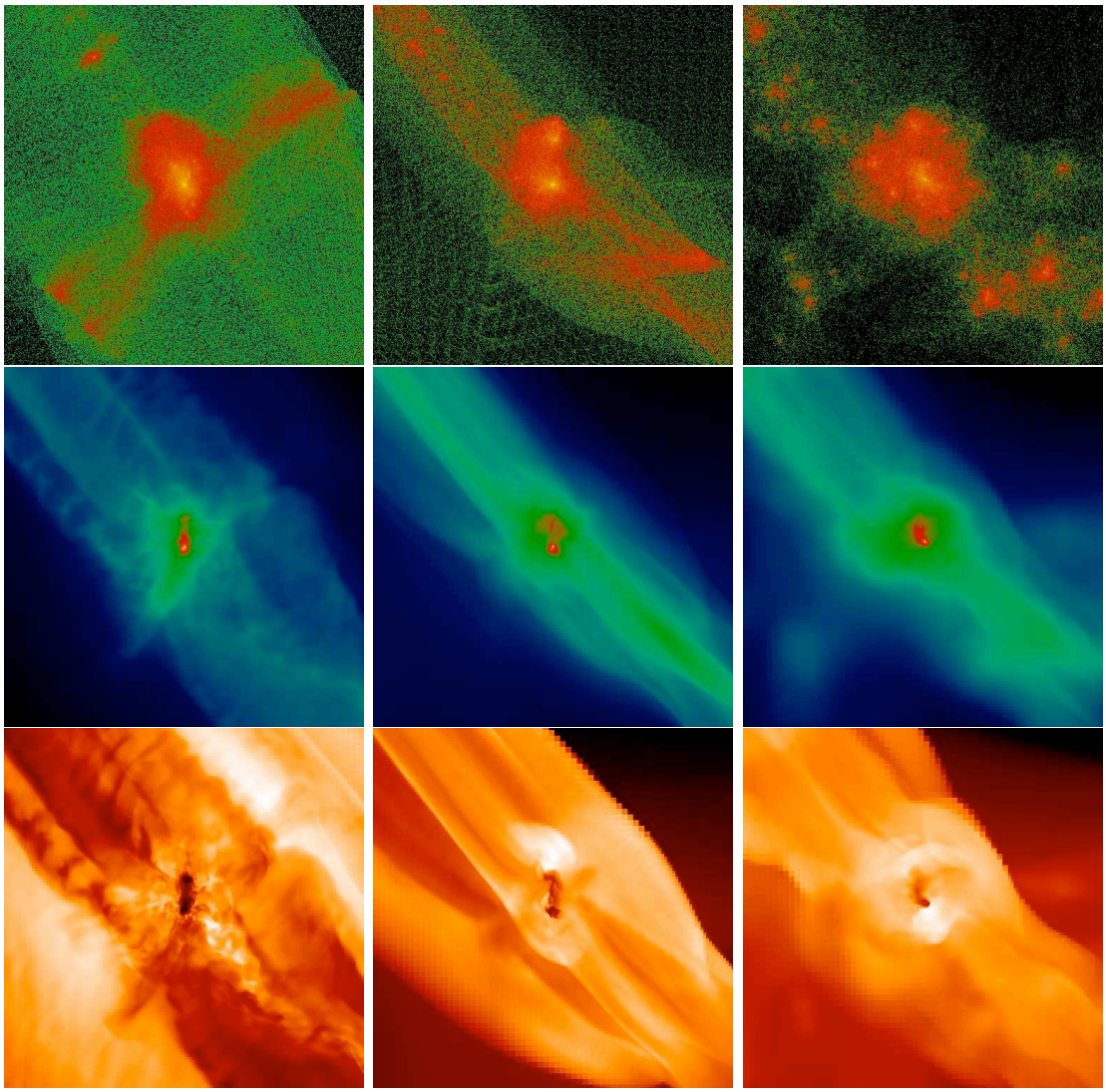

Figure 5.6: Mass-weighted projections of dark matter density, baryon density and baryon temperature for 3 simulations with the same cosmological realization and a range of warm dark matter (WDM) particle masses at the redshift at which the Population III protostar collapses in each simulation. The comoving size of the projected volume in each calculation is the same, though the color tables are relative for each panel in order to highlight density differences. Left column: $M_{WDM} = 12.5$ keV, $z_{coll} = 12.09$. Center column: $M_{WDM} = 25$ keV, $z_{coll} = 16.54$. Right column: Cold dark matter realization (corresponds to $M_{WDM} \rightarrow \infty$), $z_{coll} = 18.001$. Top row: projected dark matter density. Middle row: projected baryon density. Bottom row: projected baryon temperature. The spatial scale is ~ 300 pc (proper) for the CDM and $M_{WDM} = 25$ keV WDM simulation and ~ 450 pc (proper) for the $M_{WDM} = 12.5$ keV WDM simulation; the comoving scales are the same in each panel.

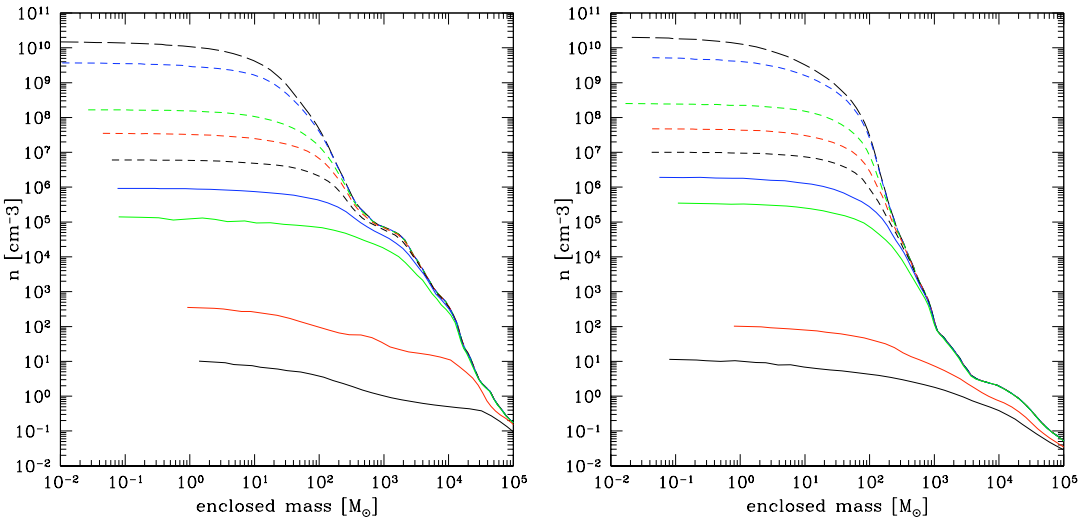

Figure 5.7: Evolution of spherically-averaged, mass-weighted baryon number density as a function of enclosed mass in halos with two representative warm dark matter simulations. The cosmological realization is the same for each calculation, and output times are chosen such that the baryon densities are approximately the same. Left column: simulation with $M_{WDM} = 12.5$ keV. Right column: simulation with $M_{WDM} = 25$ keV. The realization is the same as the simulation discussed in Section 4.4.1 and these panels are directly comparable to Figures 4.4 through 4.8. Lines for the $M_{WDM} = 12.5$ keV (25 keV) simulations as follows. Black solid line: $t = 319$ Myr/$z = 13.163$ ($t = 204$ Myr/$z = 18.05$). Red solid line: 3.12×10^7 years later (1.04×10^7 years later). Green solid line: 8.15×10^6 years later (1.04×10^6 years later). Blue solid line: $98,345$ years later (5.73×10^6 years later). Black short-dashed line: 2.86×10^5 years later (2.63×10^5 years later). Red short-dashed line: 1.25×10^5 years later ($82,433$ years later). Green short-dashed line: $45,152$ years later ($38,738$ years later). Blue short-dashed line: $22,697$ years later ($24,865$ years later). Black long-dashed line: 2691 years later (3332 years later).

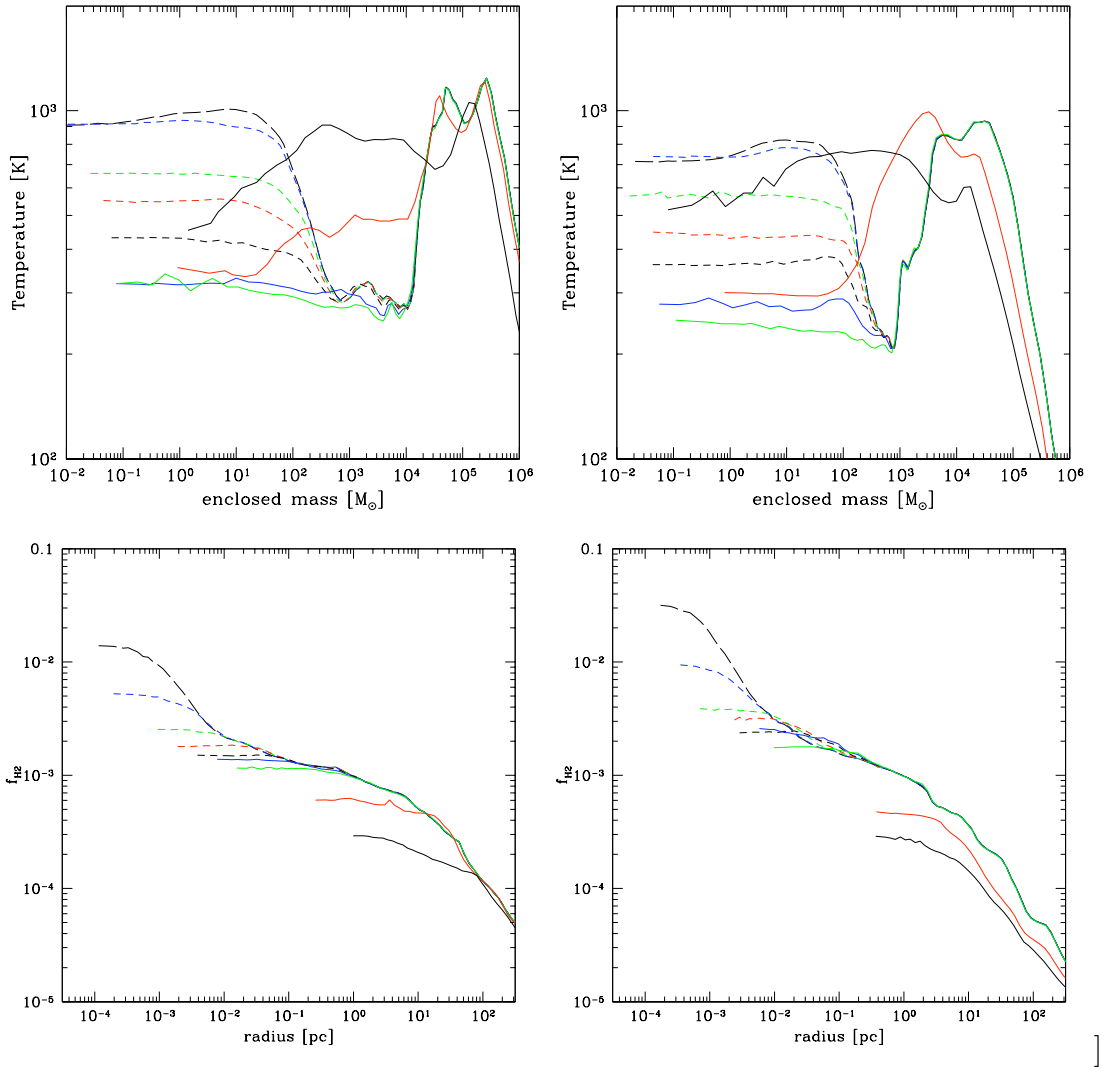

Figure 5.8: Evolution of spherically-averaged, mass-weighted baryon temperature (top row) and molecular hydrogen fraction (bottom row) as a function of enclosed mass in halos with two representative warm dark matter simulations. The cosmological realization is the same for each calculation, and output times are chosen such that the baryon densities are approximately the same. Left column: simulation with $M_{WDM} = 12.5$ keV. Right column: simulation with $M_{WDM} = 25$ keV. The realization is the same as the simulation discussed in Section 4.4.1 and these panels are directly comparable to Figures 4.4 through 4.8. The lines are at the same times as in Figure 5.7.

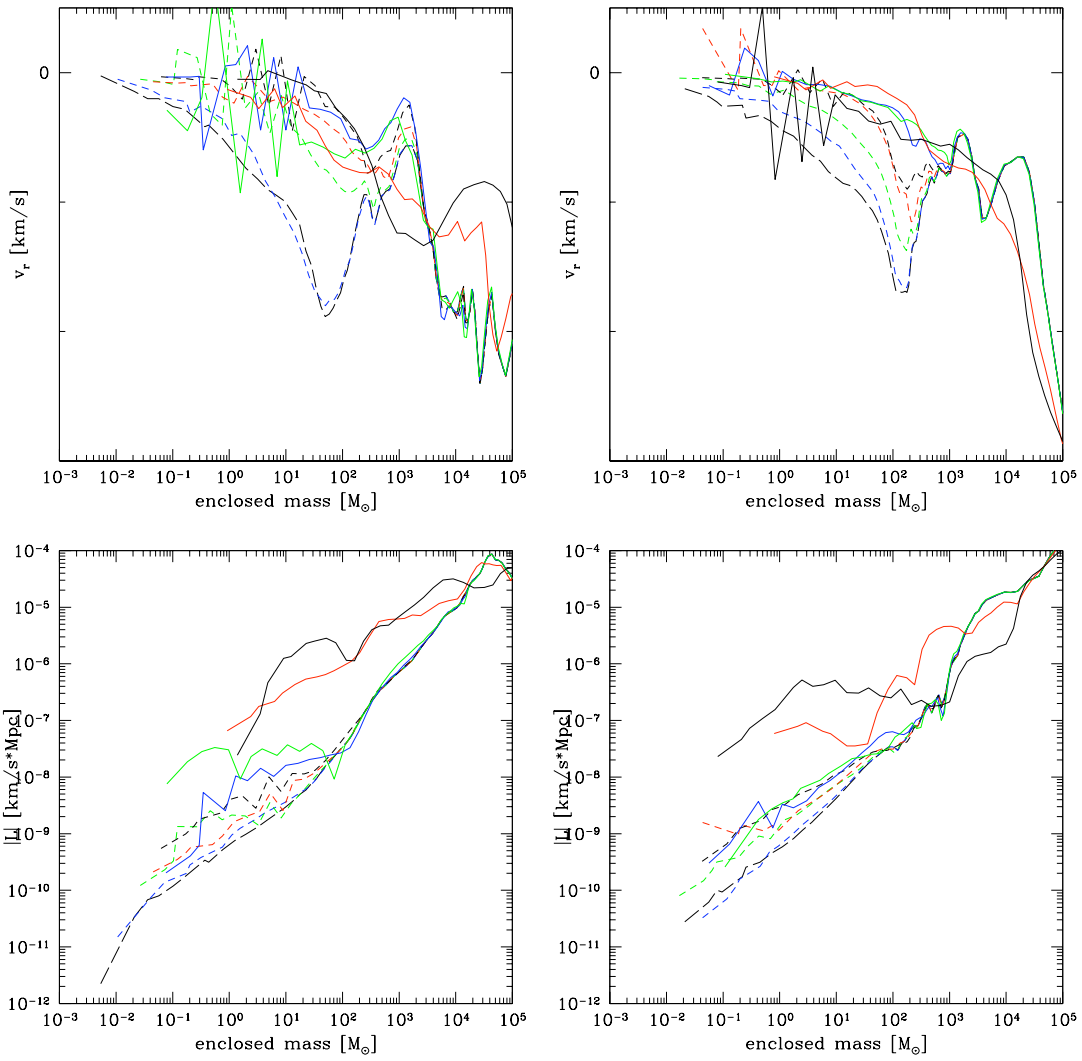

Figure 5.9: Evolution of spherically-averaged, mass-weighted baryon properties in halos with two representative warm dark matter simulations. The cosmological realization is the same for each calculation, and output times are chosen such that the baryon densities are approximately the same. Left column: simulation with $M_{WDM} = 12.5$ keV. Right column: simulation with $M_{WDM} = 25$ keV. Top row: baryon radial velocity as a function of enclosed baryon mass (velocity is positive away from the center of the halo). Bottom row: baryon angular momentum as a function of enclosed mass. The realization is the same as the simulation discussed in Section 4.4.1 and these panels are directly comparable to Figures 4.4 through 4.8. The lines are at the same times as in Figure 5.7.

the smallest object that can directly form at that mass scale. The halo that forms in the 25 keV WDM model is significantly larger than the suppression mass, implying that it formed out of the merging of smaller objects. Despite this, the final protostellar properties are similar, which is due to the collapse dynamics being controlled at small scales primarily by the properties of the primordial gas rather than by the large scale structure.

5.5 Discussion

In this chapter we show how the suppression of small-scale power, which is meant to mimic the effect of a warm dark matter cosmological model, affects the formation of a Population III protostar. We use an identical cosmological realization, but apply smoothing to the initial conditions according to the WDM transfer function given by Bode et al. We find that, for a wide range of warm dark matter particle masses, the main effect of the smoothing is to delay the collapse of the halo core, while the properties of the protostar that forms in the center of the halo remains largely unaffected, and appears to have approximately the same mass range as the reference CDM calculation.

Warm dark matter models are somewhat analogous to CDM calculations with a soft UV background, in that both cause an overall delay in collapse of the halo core and result in halos with a somewhat larger virial mass (corresponding to the later collapse time). This is due to different physical reasons, of course. One striking difference in the warm dark matter calculations is that for WDM particle masses below $\simeq$ 15 keV, the suppression mass is actually at the mass of the halo in which the primordial protostar forms (at a few times 10^5 $M_\odot$) so a different paradigm for structure formation occurs: the halos at this scale will form by town-down fragmentation of larger objects rather than bottom-up formation via hierarchical mergers.

Examination of the delay of halo collapse allows us to introduce a new constraint on the warm dark matter particle mass. A warm dark matter cosmology with a particle mass of $m_{WDM} \simeq 15$ keV delays the formation of the first star in the simulation volume by approximately 10^8 years (compared to the CDM case with the same cosmological realization). If this delay is representative of the overall delay in structure formation experienced due to small-scale smoothing from the warm dark matter then the 15 keV case is still marginally acceptable when compared against polarization measurements of the CMB from the WMAP satellite, which suggests that the universe was at least partially reionized by $z = 17 \pm 5$ [64], suggesting that a reasonable constraint on the minimum warm dark matter mass from Population III star formation is $m_{WDM} \geq 15$ keV. However, this estimate is somewhat crude, and a large number of cosmological realizations with varied warm dark matter masses should be run in order to test this hypothesis. Our simulations also show that a warm dark matter model with $m_{WDM} = 40$ keV is

indistinguishable from the CDM case, making this something of an upper limit of particle masses that have any conceivable effect on large-scale structure.